Cardiovascular Engineering and Technology (© 2022)
https://doi.org/10.1007/s13239-022-00617-3

BMES BIOMEDICAL ENGINEERING SOCIETY

Original Article

ECG Signal Quality Assessments of a Small Bipolar Single-Lead Wearable Patch Sensor

Paurakh Lal Rajbhandary, Gabriel Nallathambi, Nandakumar Selvaraj, Thang Tran, and Olivier Colliou

VitalConnect Inc., San Jose, CA, USA

(Received 21 October 2021; accepted 23 February 2022)

Abstract
Purpose—There is an increasing clinical interest in the adoption of small single-lead wearable ECG sensors for continuous cardiac monitoring. The purpose of this work is to assess ECG signal quality of such devices compared to gold standard 12-lead ECG.
Methods—The ECG signal from a 1-lead patch was systematically compared to the 12-lead ECG device in thirty subjects to establish its diagnostic accuracy in terms of clinically relevant signal morphology, wave representation, fiducial markers and interval and wave duration. One minute ECG segments with good signal quality was selected for analysis and the features of ECG were manually annotated for comparative assessment.
Results—The patch showed closest similarity based on correlation and normalized root-mean-square error to the standard ECG leads I, II, V_3 and V_4. P-wave and QRS complexes in the patch showed sensitivity (Se) and positive predictive value (PPV) of at least 99.8% compared to lead II. T-wave representation showed Se and PPV of at least 99.9% compared to lead V_3 and V_4. Mean errors for onset and offset of the ECG waves, wave durations, and ECG intervals were within 2 samples based on 125Hz patch ECG sampling frequency.
Conclusion—This study demonstrates the diagnostic capability with similar morphological representation and reasonable timing accuracy of ECG signal from a patch sensor compared to 12-lead ECG. The advantages and limitations of small bipolar single-lead wearable patch sensor compared to 12-lead ECG are discussed in the context of relevant differences in ECG signal for clinical applications.

Keywords—Bipolar lead, Electrocardiogram, ECG intervals, Lead II, P-wave, Wearable patch.

Address correspondence to Paurakh Lal Rajbhandary, VitalConnect Inc., San Jose, CA, USA. Electronic mail:

INTRODUCTION

Electrocardiogram (ECG) recording and interpretation is fundamental to current clinical practice and indispensable in the diagnosis of cardiac diseases. Clinicians rely on the morphology of ECG waveforms, presence or absence of waves, and quantification of intervals to diagnose cardiac abnormality. The modern ECG recording and monitoring technology has evolved significantly over the last few years and cardiologists may not be familiar with the impact and consequences of these technical innovations on clinical interpretation. The purpose of this paper is to provide the missing insight between the latest sensor technology and its implications on diagnostic accuracy and reliability of ECG signal quality from a clinical perspective compared to standard monitoring methods through experimental studies.

The current gold standard for ECG monitoring is based on 12-lead ECG system that requires ten electrodes to be placed on a patient's chest and/or limbs forming three limb leads (I, II, and III), three augmented leads (aVR, aVL, and aVF), and six chest leads (V_1 to V_6).[31] In hospital settings, 12-lead ECG is primarily used to diagnose cardiac disorders, study effects of different drugs, and assess functioning of implanted pacemakers.[6] 12-lead ECG are also used in pre-hospital settings, for example, by emergency personnel to assess patients with angina to identify potential acute myocardial infarction.[15] While the 12-lead ECG system provides a complete electrophysiological state of the heart, it requires longer preparation time for electrode placement,[13] any misplacement of electrodes can largely affect the signal quality,[9] the electrode wires restrict subject's movement, and movement of electrode wires can induce signal noise.

Published online: 15 March 2022

Advancement in sensor technology, integrated circuits, communication systems, and material science have opened up opportunities for monitoring of ECG using wearable sensors.[7] These miniaturized devices enable continuous monitoring of ECG for extended periods of time resulting in increased diagnostic yield.[8] Moreover, these devices have the capability to transmit the ECG in real-time, thereby enabling remote monitoring and mobile cardiac telemetry.[21] Adoption of these wearable sensors for ECG monitoring have been on the rise[3] and driven by COVID-19 pandemic, the trend can be expected to substantially increase over the next few years.

The form factor of the wearable sensor, location of device placement, choice of inter-electrode distance, orientation of the device, and selection of electrode materials can have a significant effect on the signal quality and morphology of cardiac specific signals. For example, patch-based sensors use electrodes placed in a short-distance and non-standard location. This differs from "traditional" ECG electrode technology attached in established locations on the patient's body. Differences in electrode locations, electrode materials and geometry, electrode-to-body movements, induced electrical charges due to change in contact surface, electrode distance, ion current, electrodes' frequency response, *etc*., may result in relevant differences in ECG amplitude, morphology, and timing characteristics. As a result of these technological differences from the usual ECG recorders, there is a need to systematically evaluate the quality of ECG signals from wearable patch sensors.

Research assessing ECG signal quality from the chest-based wearable patch sensor is scarce and largely limited to body surface potential mapping (BSPM) experiments where the entire thorax is covered by electrodes (e.g., upto 120 bipolar electrodes placed in a grid) to assess the smallest subset of bipolar electrodes that would provide optimal patch location considering ECG signal quality. For example, Puurtinen *et al.*[24] established that the best location for a small bipolar ECG device in terms of mean and standard deviation of the QRS-complex and the P-wave amplitudes is diagonally along the chest, with one electrode above the chest electrode location of V_1 and V_2, and the second electrode around V_2, V_3 and V_4 locations. Likewise Klum *et al.*[12] showed that signal correlation is high along the direction of the heart's electrical axis around the chest leads V_1 to V_4. In another related work, Puurtinen *et al.*[23] determined P-wave amplitude is relatively high along the direction of the electrical axis of the heart.

Unlike these prior BSPM research works that addresses the best possible location for placement of the minimally spaced electrodes, the focus of this study is the clinically important inverse problem, i.e., if a wearable sensor designed with minimally spaced ECG electrodes is placed along the electrical axis of the heart, how does its ECG signal quality compare to the 12-lead ECG system. While the BSPM studies were useful in the engineering design and development of novel single-lead wireless ECG systems, the study described here provides deeper insights into the pertinent signal differences arising from the practical realization of the electrode mapping technology and its impact on clinically relevant wave representation, ECG intervals and wave duration.

In this article, the ECG signal quality of a patch sensor with minimally spaced electrodes is systematically assessed through experimental studies by building upon the foundations set by the BPSM research on non-standard patch location. A medical-grade bipolar wearable ECG patch sensor (VitalPatch), cleared by FDA for use in home and hospital settings, with an inter-electrode distance of 7.8 cm[29] is selected in this study for quantification of ECG signal quality compared to conventional monitoring.

The main contributions of this paper are: Firstly, ECG signal morphology of the patch sensor compared to simultaneously acquired 12-lead ECG is assessed in terms of correlation and normalized root-mean-square error (RMSE). Secondly, the P-wave, QRS complex, and T-wave of the two ECG systems are manually annotated, and the sensitivity and positive predictive value of wave representation is computed. Thirdly, the onset and offset of the timing of the waves in the patch ECG are characterized and compared to lead with the best wave representation in the 12-lead ECG. Finally, the timing errors in the ECG intervals and wave durations such as PR interval, QT interval, corrected QT interval, P-wave duration, and QRS duration between the patch sensor and the reference lead of the 12-lead ECG are quantified. These results provide practical insight for clinicians on the reliability and reproducibility of the ECG signals between a small bipolar single-lead patch sensor and the 12-lead ECG device. List of all abbreviations and mathematical symbols used in this paper are enumerated in the Tables 4 and 5 in Appendix.

MATERIALS AND METHODS

VitalPatch Sensor

The VitalPatch (Fig. 1) is a small single-use fully disposable adhesive patch sensor worn on the chest with a battery life of 7 days that incorporates two hydrogel-based surface Ag/AgCl electrodes, with inter-electrode distance of 7.8 cm to measure single lead

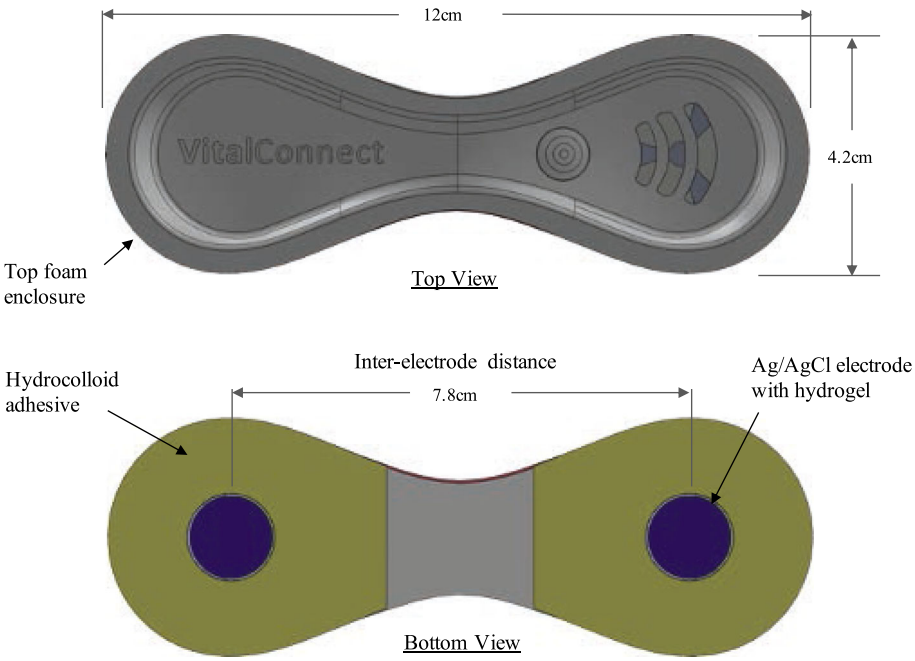

FIGURE 1. Top and bottom views of VitalPatch sensor.

bipolar ECG. The patch uses an embedded processor and Bluetooth Low Energy (BLE) transceiver for processing and transmitting the ECG signal continuously in real time. Besides ECG, the VitalPatch also continuously measures and transmits medical-grade heart rate, respiration rate, skin temperature, body temperature, steps, posture, and fall detection.[25,28,29] The mechanical design of the VitalPatch electrodes uses a similar construction to standard ECG electrodes (i.e., a combination of Ag/AgCl electrode, hydrogel, and skin adhesive). Specifically, the VitalPatch electrode consists of a flex circuit which is coated with Ag/AgCl and is covered with a hydrogel disc which makes contact with the skin. A hydrocolloid adhesive surrounds the hydrogel to secure the electrodes to the skin.

The VitalPatch is cleared by the FDA for placement on the left side of the patient's chest.[32] The recommended location of device placement is on the left chest with patch oriented at a 45-degree angle such that the upper electrode is applied two fingers below the suprasternal notch.

Experimental Setup

To assess the diagnostic accuracy and reliability of ECG signal quality of the patch sensor compared to standard monitoring, ECG signals were collected from VitalPatch and a 12-lead ECG device simultaneously for data analysis.

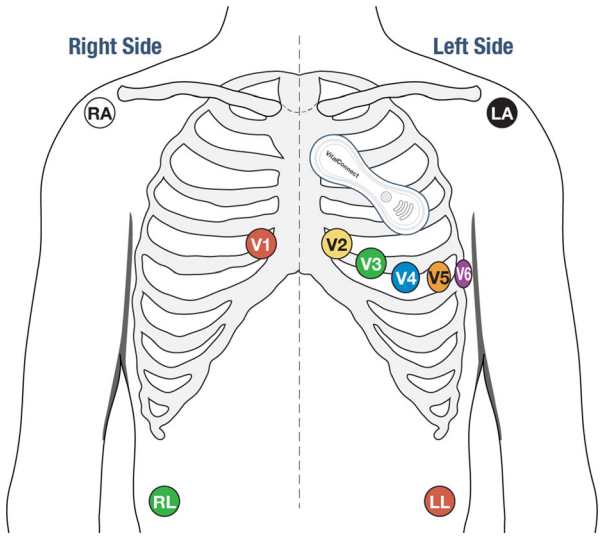

FIGURE 2. Layout of electrode placement of VitalPatch sensor and 12-lead ECG device in Mason-Likar position. RA, LA, RL, and LL are the right arm, left arm, right leg, and left leg electrodes, respectively, from which the limb leads and augmented leads are obtained.

The VitalPatch sensor was placed in the recommended location along the direction of the heart's electrical axis per the BSPM studies as shown in Fig. 2. Instructions for use were carefully followed[32] and the timestamped ECG data was transmitted to a tablet device using BLE and stored in the cloud.

The 12-lead ECG device (Cardiocard B12 10 electrode Nassiff Holter system[20]) was placed in the Mason-Likar setup as shown in Fig. 2. Mason-Likar setup

was selected in this study protocol to reduce the impact of muscle noise on the ECG signal due to limb movements. Furthermore, as the 12-lead ECG is a wired system, additional taping adhesives were used to ensure minimal effect from tugging of wires. All ECG data from the twelve leads were manually transferred and stored securely.

After initiation of data collection, the participating subjects were instructed to perform 5 min of controlled metronome breathing at six breaths per minute. This controlled breathing segment of ECG was utilized for accurate time synchronization of the two devices by a two-step process (i.e., beat level alignment based on RR-interval or RR series, which is the time difference between successive R peaks of QRS complex in the ECG, a followed by ECG sample level alignment) and the alignment was visually verified. Subjects were then instructed to stay in a stationary supine position for upto 60 min during which the signal for analysis was acquired.

In Fig. 3, a representative example of simultaneous ECG collected from a person diagnosed with a right bundle branch block using VitalPatch sensor and 12-lead ECG device is provided. The waveforms and fiducial markers of the ECG are clearly visible with good signal quality in both the patch sensor and the 12-lead device.

Data Description

Thirty subjects (15 male and 15 females) participated in the independent Institutional Review Board (IRB) approved study with informed consent. The subject characteristics are provided in Table 1 in terms of demographics, ECG intervals and wave durations.

The participating subjects comprised a wide range of age, height, weight and body mass index as detailed in Table 1. Furthermore, ECG intervals such as PR interval, QT interval, corrected QT interval by Bazett formula (QT_b), and corrected QT interval by Fridericia formula (QT_f), and wave duration such as P-wave and QRS complex duration spanned values within and outside normal limits.[14,18,26]

Data Analysis

One minute ECG segments, collected during the stationary phase and verified qualitatively as having a high signal-to-noise ratio in each of the thirty subjects, were used for the performance assessments. Four categories of ECG signal quality assessments with varying

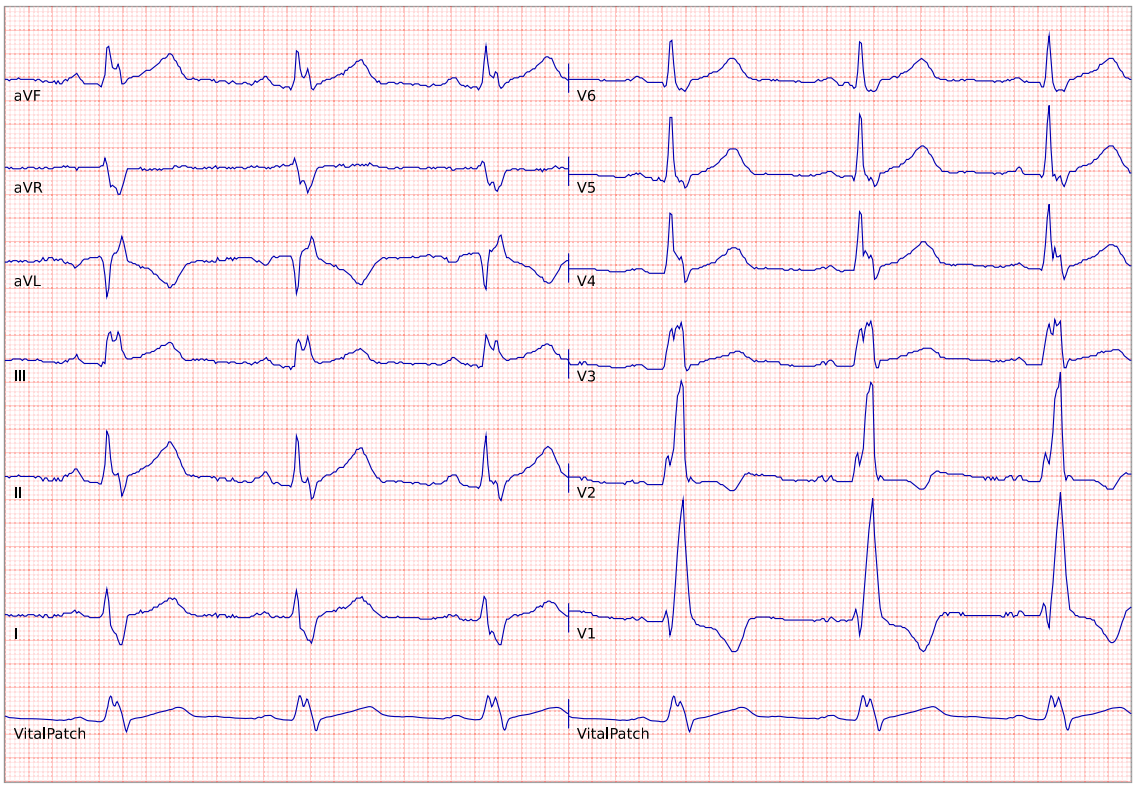

FIGURE 3. An example of simultaneous ECG signal obtained from VitalPatch sensor and 12-lead ECG device in Mason-Likar position.

TABLE 1. Subject characteristics (N = 30).

	Percentile								
Characteristics	2.5	5	10	25	50	75	90	95	97.5
Demographics									
Age (years)	24	25	27	31	36	49	54	60	62
Height (inches)	61.4	62.0	62.2	65.0	67.1	71.0	73.1	74.0	76.3
Weight (lbs)	112.5	120.0	120.0	134.5	167.0	195.0	225.0	246.0	309.0
Body mass index (kg m^{-2})	18.6	19.4	20.0	22.0	24.1	28.0	35.1	40.4	47.3
Global ECG intervals									
PR interval (ms)	104.0	112.0	120.0	136.0	144.0	160.0	184.0	192.0	216.0
QT interval (ms)	320.0	336.0	344.0	368.0	392.0	408.0	432.0	440.0	456.0
QT_b (ms)	358.2	364.0	370.1	386.7	403.5	429.1	452.0	468.8	482.2
QT_f (ms)	353.1	359.0	366.0	380.6	398.7	419.5	438.7	447.8	456.1
Global wave durations									
P-wave duration (ms)	80.0	88.0	88.0	96.0	104.0	120.0	128.0	136.0	136.0
QRS duration (ms)	88.0	88.0	96.0	96.0	104.0	112.0	120.0	128.0	128.0

levels of granularity were performed in this study and described below:

Signal Morphology Assessments

Pearson correlation coefficient ($\rho_{X,Y}$)[4] and normalized RMSE ($r_{X,Y}$)[2] were used as metrics for assessing the degree of similarity between the ECG signal morphology of VitalPatch and the leads of the 12-lead ECG as follows:

$$\rho_{X,Y} = \frac{\mathbb{E}[(X-\mu_x)(Y-\mu_y)]}{\sigma_X \sigma_Y} \tag{1}$$

and

$$r_{X,Y} = \sqrt{\frac{1}{M_s}\sum_{i=1}^{M_s}(Z_{X_i} - Z_{Y_i})^2}, \tag{2}$$

where X is the VitalPatch ECG, Y is the ECG signal of one of the leads of the 12-lead ECG, $\mathbb{E}[X]$[17] is the mathematical expected value operator of random variable X, μ is the mean, σ is the standard deviation of the signal, $Z_X = \frac{X-\mu_X}{\sigma_X}$, and M_s is the total number of samples in the signal.

The signal comparison metrics, $\rho_{X,Y}$ and $r_{X,Y}$, were calculated between the VitalPatch ECG and all possible lead combinations from the 12-lead ECG in all subjects, yielding the distribution matrices **P** and **R**, respectively. As an example, consider the case of the metric $\rho_{X,Y}$. When the correlation coefficient was computed between VitalPatch ECG and lead I in each of the N subjects from the study, a distribution vector ($P_{VP,I}$) of N correlation coefficients was generated. When the process was repeated across all leads of the 12-lead ECG, the matrix **P** consisting of twelve distribution vectors with each of them having N data points was generated as follows:

$$\mathbf{P} = \begin{bmatrix} \rho^{1}_{VP,V_6} & \rho^{2}_{VP,V_6} & \cdots & \rho^{N}_{VP,V_6} \\ \rho^{1}_{VP,V_5} & \rho^{2}_{VP,V_5} & \cdots & \rho^{N}_{VP,V_5} \\ \vdots & \vdots & \ddots & \vdots \\ \rho^{1}_{VP,I} & \rho^{2}_{VP,I} & \cdots & \rho^{N}_{VP,I} \end{bmatrix} = \begin{bmatrix} \mathbf{P}_{VP,V_6} \\ \mathbf{P}_{VP,V_5} \\ \vdots \\ \mathbf{P}_{VP,I} \end{bmatrix}. \tag{3}$$

Wilcoxon signed rank test was then computed to evaluate the null hypothesis that $|P_{VP,i}|$ (absolute value of the correlation coefficient of lead pair VitalPatch and lead I of 12-lead) is less than or equal to $|P_{VP,j}|$ (absolute value of the correlation coefficient of lead pair VitalPatch and lead j of 12-lead ECG), i.e., $|P_{VP,i}| \leq |P_{VP,j}|$. All possible statistical comparisons of the hypothesis testing represented by the matrix

$$\mathbf{H}_\rho = \begin{bmatrix} \mathbf{H}^{V_6,I}_\rho & \mathbf{H}^{V_6,II}_\rho & \ldots & \mathbf{H}^{V_6,V_6}_\rho \\ \mathbf{H}^{V_5,I}_\rho & \mathbf{H}^{V_5,II}_\rho & \ldots & \mathbf{H}^{V_5,V_6}_\rho \\ \vdots & \vdots & \ddots & \vdots \\ \mathbf{H}^{I,I}_\rho & \mathbf{H}^{I,II}_\rho & \ldots & \mathbf{H}^{I,V_6}_\rho \end{bmatrix} \tag{4}$$

was used to rank the degree of similarity based on the correlation coefficient of the VitalPatch ECG compared to each of the leads of the 12-lead ECG. $\mathbf{H}^{i,j}_\rho$ = p-value for null-hypothesis: $|P_{VP,i}| \leq |P_{VP,j}|$ tested with $\alpha = 0.05$. As $\rho_{X,Y}$ is a signed metric ranging from -1 to 1, $P_{VP,i}$ that spans both positive and negative values, it is excluded from hypothesis testing.

Similarly, the matrix **R** is obtained by calculating $r_{X,Y}$ between VitalPatch ECG and each of the leads of the 12-lead ECG. $R_{VP,i}$ is computed similar to Eq. (3) with RMSE. There is no exclusion criterion for $R_{VP,i}$ as $r_{X,Y}$ is always non-negative. The Wilcoxon signed rank test was then computed to evaluate the null hypothesis that $R_{VP,i} \geq R_{VP,j}$, and the $\mathbf{H_r}$ matrix was obtained by

repeating the process across all possible statistical comparisons of the hypothesis testing as follows:

$$\mathbf{H_r} = \begin{bmatrix} \mathbf{H_r^{V_6,I}} & \mathbf{H_r^{V_6,II}} & \dots & \mathbf{H_r^{V_6,V_6}} \\ \mathbf{H_r^{V_5,I}} & \mathbf{H_r^{V_5,II}} & \dots & \mathbf{H_r^{V_5,V_6}} \\ \vdots & \vdots & \ddots & \vdots \\ \mathbf{H_r^{I,I}} & \mathbf{H_r^{I,II}} & \dots & \mathbf{H_r^{I,V_6}} \end{bmatrix}, \quad (5)$$

where $H_r^{i,j} = p$value for null-hypothesis: $R_{\mathrm{VP,i}} \geq R_{\mathrm{VP,j}}$ tested with $\alpha = 0.05$.

Wave Representation Assessments

Beat-by-beat comparison of ECG from leads of 12-lead ECG and VitalPatch was performed. Peaks of P-wave, QRS-complex (R-wave peaks) and peaks of T-wave were manually annotated in 12-lead device and VitalPatch independently to assess the ability of the patch sensor to accurately capture depolarization of atria (P-wave), depolarization of the ventricles (QRS complex) and the repolarization of the ventricles (T-wave). The detection performance metrics were calculated in terms of sensitivity (Se), positive predictive value (PPV) and F1-score[22] assuming the signal in the selected lead of 12-lead ECG is the ground truth.

$$\mathrm{Se} = \frac{\mathrm{TP}}{\mathrm{TP} + \mathrm{FN}}, \quad (6)$$

$$\mathrm{PPV} = \frac{\mathrm{TP}}{\mathrm{TP} + \mathrm{FP}} \text{ and} \quad (7)$$

$$\text{F1-score} = 2 \times \frac{\mathrm{Se} \times \mathrm{PPV}}{\mathrm{Se} + \mathrm{PPV}}, \quad (8)$$

where TP, FP, and FN are true positives, false positives, and false negatives, respectively.

Fiducial Marker Assessments

Exact timing of fiducial markers such as onset of P-wave and QRS-complex, and offset of P-wave, QRS-complex and T-wave were manually annotated in the 12-lead device and VitalPatch independently to quantify the accuracy of delineating these characteristic points in the patch sensor. The delineation performance metric was assessed in terms of timing error of fiducial markers (f) between 12-lead device and VitalPatch, where the mean error for a subject was calculated as timing in VitalPatch ECG ($t_{\mathrm{VP,f}}$) subtracted from corresponding parameter of the reference lead of 12-lead ECG ($t_{\mathrm{12L,f}}$), i.e., $t_{\mathrm{E,f}} = \frac{1}{M_\mathrm{f}} \sum_{k=1}^{M_\mathrm{f}} t_{\mathrm{12L,k}} - t_{\mathrm{VP,k}}$, with f being the fiducial marker such as onset and offset of P-wave, QRS-complex, and T-wave, and M_f is the total number of pairwise annotations of a fiducial marker in a subject.

ECG Interval and Wave Duration Assessments

Finally, the clinically useful intervals and durations such as PR-interval, RR interval (RR), QT interval, corrected QT intervals ($\mathrm{QT_b} = \frac{\mathrm{QT}}{\sqrt{\mathrm{RR}}}$ and $\mathrm{QT_f} = \frac{\mathrm{QT}}{\sqrt[3]{\mathrm{RR}}}$), P-wave duration, and QRS duration were manually annotated in 12-lead device and VitalPatch independently to compute the accuracy of characterizing the ECG intervals and wave durations in the patch sensor. The performance was assessed in terms of timing error of interval/duration measurements between 12-lead device and VitalPatch, where the mean error in intervals and durations was calculated as parameters being analyzed (interval or duration) in VitalPatch ECG ($t_{\mathrm{VP},i}$) subtracted from the corresponding parameter of the reference lead of 12-lead ECG ($t_{\mathrm{12L},i}$) i.e., $t_{\mathrm{E},i} = \frac{1}{M_i} \sum_{k=1}^{M_i} t_{\mathrm{12L},k} - t_{\mathrm{VP},k}$, with i being the ECG intervals/wave duration such as PR-interval, QT interval, corrected QT intervals, P-wave duration, and QRS duration, and M_i is the total number of samples of an interval or duration parameter in a subject.

Manual Annotation

The features of ECG such as peak locations of waves, onset and offset of fiducial markers, ECG intervals and wave durations that were manually annotated is graphically illustrated in Fig. 4. As the manual annotation is a laborious and time-consuming process, it is subdivided into different stages. In the first stage, annotation was performed based on the results of signal morphology assessments. Out of the 12-leads, two limb leads and two bipolar chest leads that were closest to the VitalPatch ECG in terms of $\rho_{X,Y}$ and $r_{X,Y}$ were selected for further annotation of peaks of P-wave, QRS-complex and T-wave. In the second stage, granular annotation of the onset and offset of fiducial markers, ECG intervals and duration of the waves was performed for the lead showing the best wave representation, especially in terms of the P-wave and QRS complex.

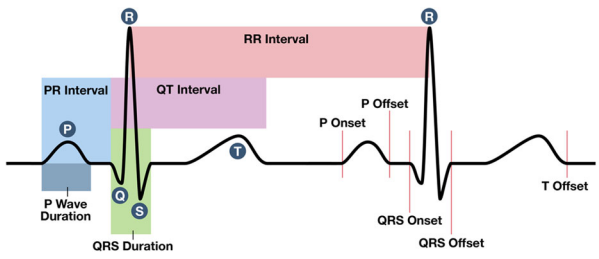

FIGURE 4. Illustration of features of ECG that were manually annotated in the VitalPatch and the 12-lead device.

RESULTS

Characterization of Signal Morphology

The outcome of the Wilcoxon rank sum test for correlation coefficient ($\mathbf{H_p}$ matrix) is shown in Fig. 5a. Leads III, aVL, and V_1 were excluded from the hypothesis testing as $\rho_{X,Y}$ span both positive and negative values in these leads. Lead I and lead II demonstrated a significantly ($p \leq 0.05$) higher magnitude of correlation coefficient between the ECG signal morphology of VitalPatch and the limb leads of the 12-lead ECG. Likewise, lead V_3 and lead V_4 demonstrated a significantly ($p \leq 0.05$) higher magnitude of correlation coefficient between the ECG signal morphology of VitalPatch and the bipolar chest leads of the 12-lead ECG.

The outcome of the Wilcoxon rank sum test for normalized RMSE ($\mathbf{H_r}$ matrix) is shown in Fig. 5b. Leads I and II among the limb leads, and leads V_3 and V_4 among the bipolar chest leads demonstrated a significantly ($p \leq 0.05$) lower normalized RMSE between the ECG signal morphology of VitalPatch and the leads of the 12-lead ECG.

Typical ECG signal from VitalPatch with concurrent leads I, II, V_3 and V_4 of 12-lead ECG during the stationary phase of the subject is shown in Fig. 6. While differences in absolute amplitude are expected due to differences in inter-electrode distance, all key features of the ECG such as P-wave, QRS complex, and T-wave are clearly visible in the patch sensor. Based on the signal morphology assessments, leads I, II, V_3 and V_4 of 12-lead ECG were selected for further quantitative characterization of wave representation as they show higher correlation and lower normalized RMSE than other leads when compared to the VitalPatch ECG.

Characterization of Wave Representation

Wave representation statistics in terms of Se, PPV and F1-score are provided in Table 3. As expected, the QRS complex of the ECG signal from the patch sensor was well represented compared with each of the four selected leads I, II, V_3 and V_4. The total positives were slightly different across the four leads when compared with the VitalPatch ECG as any beat during a segment with discernible noise in VitalPatch or one of the four leads of 12-lead perceived as noise was excluded from the analysis. Among the four leads, leads II and V_4 showed higher representation of the QRS complex unaffected by noise.

Of significant interest for arrhythmia diagnosis is the representation of P-wave (atrial depolarization) in the patch sensor. The highest representation of the P-wave with the least false positives was observed in lead II, while a relatively lower representation of the P-wave with higher false positives was seen in lead I. False positive cases arise when P-waves were not visible in a particular channel of the 12-lead ECG due to obfuscation by the noise floor but were observed in the ECG of the patch sensor. Analysis of the false positives for the P-wave showed that they predominantly occurred in some leads of a few subjects due to poor amplitude resolution. As an example, consider the case of the 53 false positives in P-wave representation in VitalPatch ECG compared to lead I. Root-cause analysis showed that while P waves were clearly visible in VitalPatch and leads such as II, V_3 and V_4, lead I did not show discernable P-waves due to poor amplitude resolution below the noise floor. Hence, most of the false positives were a consequence of assuming the wave representation in each of the 12-leads was the ground truth and, in a physiological sense, they were not exactly false positives. Similar observations were found for the false positive cases for the T-wave representation in VitalPatch ECG compared to lead II (Table 2).

Lead II of 12-lead ECG was selected for further characterization of fiducial markers, ECG intervals, and wave durations as it showed the best wave representation compared to the ECG of VitalPatch, especially considering the depolarization of atrial and ventricles.

Characterization of Fiducial Markers, ECG Intervals, and Wave Durations

The timing error statistics of onset and offsets of the waves, ECG intervals, and wave durations between VitalPatch ECG and lead II of 12-lead ECG is shown in Table 3. On average, the offset of QRS complex and T-wave occurred earlier in lead II compared to VitalPatch, while the onset and offset of P-wave occurred earlier in VitalPatch compared to lead II. Additionally, at a patch ECG sampling frequency of 125 Hz, the average error for onset and offset of QRS complex and offset of P-wave was within 1-ECG sample, while the average error of onset of P-wave and offset of T-wave were within 2-ECG samples.

Finally, the average error for duration of P-wave and QRS complex was within the 1-ECG sample, while the average error of PR interval, QT interval, and corrected QT intervals were within 2-ECG samples.

DISCUSSION

Use of wearable sensors for remote patient monitoring is an emerging trend and is being increasingly adopted in continuous and ambulatory settings for

(a)

	I	II	III	aVR	aVL	aVF	V1	V2	V3	V4	V5	V6
V6	1	0.98	-	1	-	0.088	-	0.273	0.999	1	1	1
V5	0.979	0.019	-	0.742	-	0	-	0.021	0.967	1	1	0
V4	0.027	0	-	0.001	-	0	-	0	0.296	1	0	0
V3	0.074	0.009	-	0.032	-	0.002	-	0	1	0.712	0.035	0.001
V2	0.997	0.828	-	0.959	-	0.621	-	1	1	1	0.98	0.734
V1	-	-	-	-	-	-	1	-	-	-	-	-
aVF	1	1	-	1	-	1	-	0.388	0.998	1	1	0.916
aVL	-	-	-	-	1	-	-	-	-	-	-	-
aVR	0.845	0	-	1	-	0	-	0.043	0.97	0.999	0.266	0
III	-	-	1	-	-	-	-	-	-	-	-	-
II	0.998	1	-	1	-	0	-	0.178	0.991	1	0.982	0.021
I	1	0.002	-	0.161	-	0	-	0.003	0.929	0.974	0.022	0

(b)

	I	II	III	aVR	aVL	aVF	V1	V2	V3	V4	V5	V6
V6	1	0.919	0	0	0	0.013	0	0.103	0.999	1	1	1
V5	0.663	0.004	0	0	0	0	0	0.001	0.971	1	1	0
V4	0.001	0	0	0	0	0	0	0	0.244	1	0	0
V3	0.021	0.003	0	0	0	0	0	0	1	0.763	0.03	0.001
V2	0.998	0.929	0.054	0	0	0.646	0	1	1	1	0.999	0.901
V1	1	1	1	0	0.86	1	1	1	1	1	1	1
aVF	1	1	0	0	0	1	0	0.362	1	1	1	0.988
aVL	1	1	0.98	0	1	1	0.145	1	1	1	1	1
aVR	1	1	1	1	1	1	1	1	1	1	1	1
III	1	1	1	0	0.021	1	0	0.948	1	1	1	1
II	0.993	1	0	0	0	0	0	0.074	0.997	1	0.997	0.084
I	1	0.008	0	0	0	0	0	0.002	0.98	0.999	0.345	0

FIGURE 5. Hypothesis testing for VitalPatch ECG compared to leads of 12-lead ECG. (a) H_ρ matrix (see Eq. (4)). (b) H_r matrix (see Eq. (5)). The white background fields represent the rejection of the null hypothesis and '-' represents the fields excluded from hypothesis testing.

enhanced patient care and management. Currently, wearable sensors are not only replacing older ECG technology in established markets such as holter monitors, event monitors, and mobile cardiac telemetry,[1] but also creating new monitoring paradigms such as hospital-level care at home.[27] One of the key questions that remains as a detriment to widespread clinical adoption of miniaturized wearable devices is how well do ECG from these devices with smaller inter-electrode distance and non-standard device placement location compare to traditional ECG signals. In this article, we address this crucial question by comparing an ECG

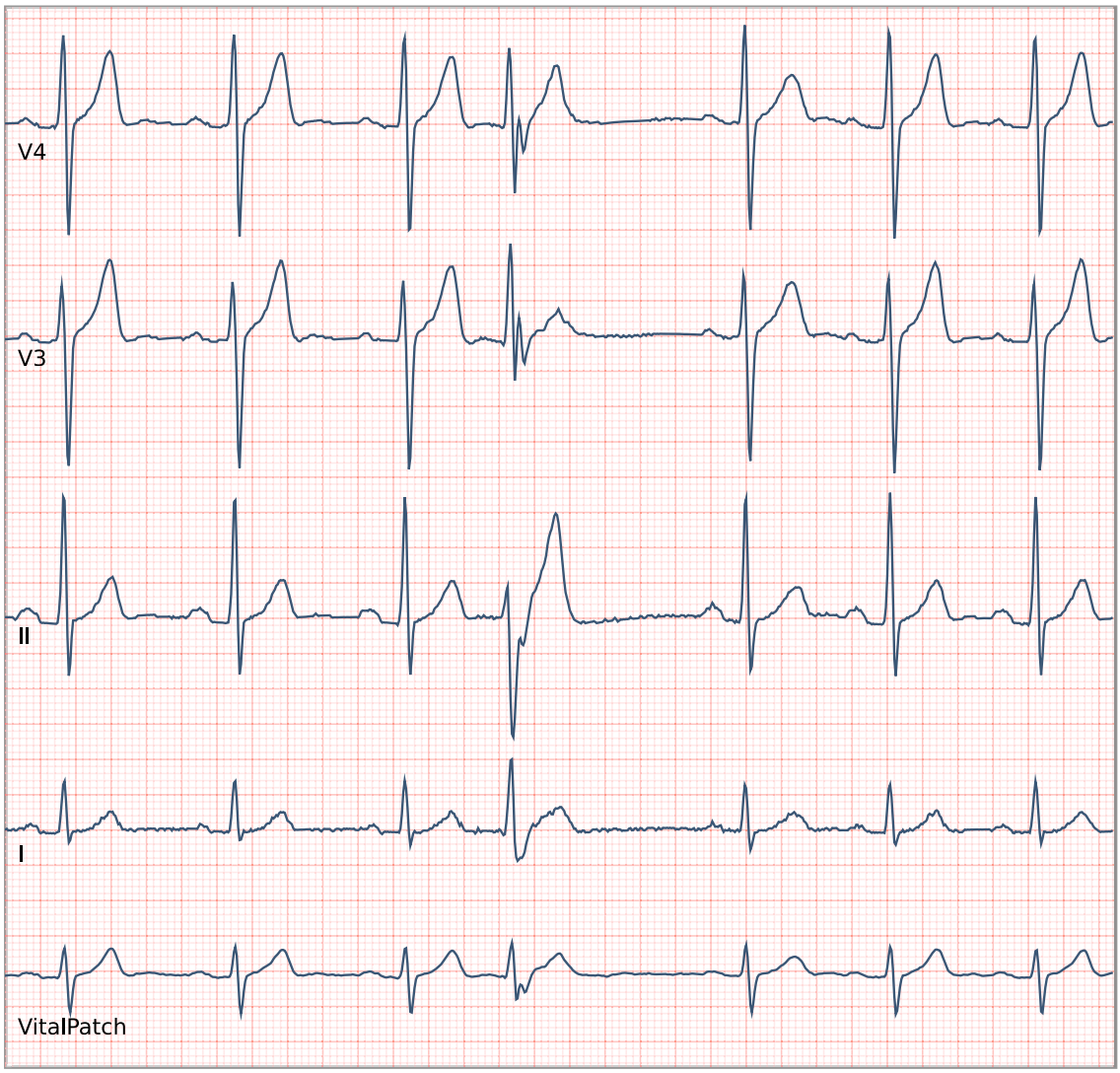

FIGURE 6. Representative ECG signal with an ectopic beat from leads I, II, V_3 and V_4 of 12-lead ECG that are closest to the VitalPatch in terms of correlation coefficient and normalized Root Mean Square Error (RMSE).

TABLE 2. Wave representation of ECG of VitalPatch compared to leads I, II, V_3 and V_4 of 12 lead ECG.

Waveform	Lead	TP	FP	FN	Se (%)	PPV (%)	F1-score (%)
QRS complex	I	1789	0	0	100.0	100.0	100.0
	II	1824	0	0	100.0	100.0	100.0
	V_3	1784	0	0	100.0	100.0	100.0
	V_4	1822	0	0	100.0	100.0	100.0
P-wave	I	1732	53	1	99.9	97.0	98.5
	II	1816	4	2	99.9	99.8	99.8
	V_3	1777	3	1	99.9	99.8	99.9
	V_4	1800	18	1	99.9	99.0	99.5
T-wave	I	1757	1	0	100.0	99.9	100.0
	II	1713	79	0	100.0	95.6	97.7
	V_3	1754	0	0	100.0	100.0	100.0
	V_4	1791	2	0	100.0	99.9	99.9

TP true positive, *FP* false positive, *FN* false negative, *Se* sensitivity, *PPV* positive predictive value, *F1-score* harmonic mean of Se and PPV.

TABLE 3. Fiducial markers, ECG intervals, and wave durations of VitalPatch ECG compared to lead II (all values are provided as mean ± standard deviation).

Fiducial markers	
Characteristics	$t_{E,f}$ (ms)
P-onset	− 8.5 ± 8.2
P-offset	− 4.5 ± 7.4
QRS-onset	− 0.6 ± 6.7
QRS-offset	2.7 ± 6.9
T-offset	11.0 ± 7.8
ECG interval and wave durations	
Characteristics	$t_{E,i}$ (ms)
P-wave duration	4.2 ± 8.5
QRS duration	3.4 ± 8.7
PR interval	8.3 ± 9.5
QT Interval	11.0 ± 9.7
QT_b	12.1 ± 11.0
QT_f	11.9 ± 10.8

$t_{E,f}$ and $t_{E,i}$ are mean timing error of a ECG fiducial marker(f) and interval/duration(i) calculated as difference of VitalPatch ECG from 12-lead ECG.

signal from a patch sensor placed along the direction of the electrical axis of the heart with simultaneously acquired 12-lead ECG to provide a comprehensive analysis of the differences in the signal characteristics from both non-clinical and clinical perspectives.

In-depth analysis of non-clinical assessment presented in this paper includes statistical tests of significance based on Pearson correlation coefficient and normalized RMSE that provide an indication of the order of similarity between non-standard patch ECG and the different leads of the 12-lead ECG. While prior BSPM work by Klum *et al.*[12] indicated maximal correlation was found between minimally spaced electrodes placed diagonally on the left side of the chest spanning 2nd to 4th intercostal rib, the present study extends the results to show that the patch sensor placed along the electrical axis of the heart has significantly ($p \leq 0.05$) higher correlation (and lower normalized RMSE) in specific leads I, II, V_3 and V_4 compared to other leads of the 12-lead ECG. Although the normalized RMSE and correlation coefficient provide an assessment of signal comparison that is easy to interpret, it is challenging to translate these results in the clinical context. Furthermore, these metrics, by definition, weights equally all data points in the signal including redundant periods such as isoelectric deviations, which may not be clinically relevant from the perspective of ECG signal quality.

To fully discriminate clinically relevant aspects of the ECG signal quality, metrics based on presence or absence of the different ECG waves, fiducial markers representing onset and offset of these waves, and ECG intervals and wave durations derived from these markers are presented in this study. Although annotation of these characteristic markers for analysis is a laborious process, it is necessary to provide an objective assessment of the diagnostic accuracy and reliability of ECG signal quality from a clinical perspective.

The patch sensor showed an excellent representation of the pertinent waves of the ECG signal such as QRS complex, P-wave and T-wave. Specifically, the representation of the P-wave and QRS complex in the patch sensor is similar to lead II with Se and PPV of at least 99.8% while the representation of T-wave is similar to the bipolar leads V_3 and V_4 with Se and PPV of at least 99.9%. It should be noted that the patch sensor is very robust to noise compared to the 12-lead ECG, as evidenced by the incidence of false positives in some of the leads. In fact, the patch sensor manifests the best wave representation of both limb leads (as shown by the total positives of P-wave and QRS complex in lead II) and bipolar chest leads (as shown by the total positives of T-wave in V_4). The relatively lower incidence of noise in the patch sensor may be a consequence of the absence of wires tugging on the electrodes and minimal electrode-to-body movements due to patch geometry.

The fiducial marker analysis comparing the onset and offset of these waves is clinically significant to understand the cardiac electrophysiology and conduction process. The results show that the mean error of onset and offset of P-waves occur earlier in VitalPatch with shorter P-wave durations compared to lead II. In general, all ECG intervals and wave intervals are relatively shorter in the VitalPatch compared to lead II. While this may be a direct consequence of the inter-electrode distance, non-standard location, and electrode geometry, it is also influenced by the sampling frequency of the ECG signal. Typically, the patch sensors are wireless and battery operated and utilize a lower sampling frequency to reduce processing and transmission power consumption, thereby prolonging the battery life of the device. However, this tradeoff affects the timing resolution of the ECG intervals and wave duration to some extent.

The main limitations of the study include the sample size of patients and the inter/intra observer variability in the placement of the electrodes. In this study, a patient population of 30 subjects were used, and within each subject 1800 beats were analyzed across all channels of the 12-lead device and the patch sensor, corresponding to 63,000 features of ECG that were manually annotated. While increasing subject cohort size to a wider range of demographics and conditions increases the statistical power of the study, due to the challenges and time constraints involved in careful annotation and verification of all fiducial markers, the patient population was limited to 30 subjects in this

study.Future studies may extend to a larger subject cohort. Additionally, ECG signal quality may be affected by misplacement or variability of placement of electrodes across and within study coordinators.[11] While care was taken to consistently place the electrodes in the correct position per standard clinical practice, inter and intra operator variability may have an impact on the placement of electrodes, and those variations are not quantified in this study.

Overall, the results show the diagnostic capability of ECG signal from patch sensor with reduced noise burden and reasonable timing accuracy compared to 12-lead ECG. The small size and real-time wireless ECG data transmission of the patch sensor enhance its comfort and wearability, which translate into the possibility of long term ambulatory monitoring.[1,27,30] Unlike the 12-lead ECG monitoring method, which requires placement of 10 wired electrodes with increased patient discomfort and reduced compliance, the patch sensor provides the patient with a miniaturized, wireless, and comfortable ambulatory sensor, which is well suited for use in remote patient monitoring settings. Finally, in addition to ECG monitoring, these patch sensors are often enhanced with vital signs and activity monitoring algorithms, thereby increasing the range of healthcare applications.

Despite these advantages, the patch sensor with minimal inter-electrode distance and non-standard locations has some limitations. As patch sensors are often single-lead ECG devices with relatively lower amplitudes, the origin of arrhythmia cannot be localized. The ECG intervals measured by patch sensor are strictly lead intervals as opposed to the capability of measuring global intervals (which relies on the earliest onset and latest offset of fiducial markers among the leads) in a 12-lead device. The ECG interval monitoring for critical applications (e.g., monitoring of QT interval during the initiation of antiarrhythmic therapy) and heart rate variability studies[16] often require high timing resolution which may not be obtained due to limitations in sampling frequency of the patch sensor. Another consequence of the relatively lower sampling frequency is the inability of the patch sensors to accurately display pacemaker pulses, which require a sampling frequency of at least 4 kHz.[19]

While the patch sensor may not fully replace diagnostic 12-lead ECG in critical patient monitoring, there are many applications that benefit from the advances in patch ECG technology. As the patch sensors are unobtrusive, they increase the mobility of patients by allowing them to move freely outside the confines of the hospital bed. The multi-functional monitoring capability of the wireless patch sensors enables continuous monitoring of vital signs, activity, and arrhythmia for extended periods of time in both hospital and home settings. Real-time remote patient monitoring with the patch sensor can be used to alleviate the strain on hospital resources by allowing patients to be cared for at home. The COVID-19 pandemic has also accelerated the interest in using wireless patch sensors for cardiac monitoring as it reduces exposure of the health providers to the virus by enabling remote patient monitoring.[5,10] Finally, the patch sensors that are fully disposable eliminates both the need for disinfecting the device and the risk of cross contamination. Because of these benefits, an increase in the usage of these patch sensors in appropriate clinical situations can be anticipated.

The present study provides a solid foundation on the relevant differences in ECG signal due to latest advances in wearable sensor technology in terms of waveforms, ECG intervals and wave durations. The results demonstrate the reproducibility, reliability and diagnostic accuracy of a small bipolar single-lead patch sensor compared to a 12-lead ECG device. Future studies in this direction that focus on understanding and characterizing the specific wave patterns (e.g., QRS fragmentation patterns for conduction disorders such as left and right bundle branch block) in the small bipolar chest lead compared to standard patterns of manifestation in 12-lead ECG recorders will be of huge benefit to the electrophysiology community.

ACKNOWLEDGMENTS

The authors acknowledge Frank Stelter and Anagha Desai for assisting in the graphics and data collection, respectively.

CONFLICT OF INTEREST

Author PLR, during the time of involvement in this work, was employed by and received salary and stock options from VitalConnect Inc. Author GN is employed by and received salary and stock options from VitalConnect Inc. Author NS, during the time of involvement in this work, was employed by and received salary and stock options from VitalConnect Inc. Author TT is employed by and received salary and stock options from VitalConnect Inc. Author OC is employed by and received salary and stock options from VitalConnect Inc. The presented study is funded by VitalConnect Inc.

APPENDIX

See Tables 4 and 5

TABLE 4. List of abbreviation and their definitions.

Abbreviation	Definition
BLE	Bluetooth Low Energy
BSPM	Body Surface Potential Map
ECG	Electrocardiogram
FN	False Negative
FP	False Positive
IRB	Institutional Review Board
PPV	Positive Predictive Value
RMSE	Root Mean Square Error
Se	Sensitivity
TP	True Positive

TABLE 5. List of symbols and their definitions.

Symbol	Description
avL, avR, avF	Augumented limb leads (augmented vector left, augmented vector right, and augmented vector foot respectively) of 12-lead ECG
$E[X]$	Mathematical expeced value operator of random variable X
f	Fiducial markers of the ECG signal
F1-score	Harmonic mean of Se and PPV
$\mathbf{H}_\mathrm{r}$	Normalized RMSE based hypothesis test matrix with each element showing the p value of the null hypothesis
$\mathbf{H}_\rho$	Correlation coefficient based hypothesis test matrix with each element showing the p value of the null hypothesis
$H_\rho^{i,j}$	p value of null hpyothesis $\lvert P_{\mathrm{VP},i}\rvert \leq \lvert P_{\mathrm{VP},j}\rvert$
$H_\mathrm{r}^{i,j}$	p value of null hpyothesis $R_{\mathrm{VP},i} \geq R_{\mathrm{VP},j}$
I–III	Limb leads of 12-lead ECG
M_f	Total number of pairwise annotations of a fiducial marker in a subject
M_i	Total number of pairwise annotations of a ECG interval or durations in a subject
M_s	Total number of samples in the signal
N	Total number of subjects in the study
$\mathbf{P}$	Distribution matrix formed by row-wise stacking of distribution vector $P_{\mathrm{VP},i}$
$P_{\mathrm{VP},i}$	Distribution row vector of N correlation coefficients computed between ECG of VitalPatch and ith lead of 12-lead ECG
p value	The probability of obtaining test results at least as extreme as the results actually observed, under the assumption that the null hypothesis is correct, when tested using Wilcoxon Signed Rank Test
PR	PR interval measured as time between onset of P wave and onset of QRS complex in ECG
QRS	QRS interval duration measured as time between onset of Q wave to the and offset of S wave in ECG
QT	QT interval measured as time between onset of Q-wave to and offset of T-wave in ECG
$\mathrm{QT_b}$	Corrected QT interval by Bazett formula
$\mathrm{QT_f}$	Corrected QT interval by Fredericia formula
$\mathbf{R}$	Distribution matrix formed by row-wise stacking of distribution vector $R_{\mathrm{VP},i}$
$R_{\mathrm{VP},i}$	Distribution row vector of N normalized RMSE values computed between ECG of VitalPatch and ith lead of 12-lead ECG
$r_{X,Y}$	Normalized root mean squared error between X and Y
RR	RR interval measured as time between two successive R peaks of QRS complex in ECG signal
$t_{\mathrm{E,f}}$	Timing error of a fiducial marker (such as onset and offset of ECG waves) calculated as difference of VitalPatch ECG from 12-lead ECG
$t_{\mathrm{E},i}$	Timing error of a ECG interval/duration (such as PR interval, QRS duration, *etc.*) calculated as difference of VitalPatch ECG from 12-lead ECG
$t_{\mathrm{12L,f}}$	Timing of fiducial marker f in 12 Lead ECG
$t_{\mathrm{VP,f}}$	Timing of fiducial marker f in VitalPatch ECG
$t_{\mathrm{12L},i}$	Timing of ECG interval or duration i in 12 Lead ECG
$t_{\mathrm{VP},i}$	Timing of ECG interval or duration i in VitalPatch ECG
$V_1 - V_6$	Chest leads of 12-lead ECG
Z_X	Z-score normalization of variable X
μ_X	Mean value of variable X
$\rho_{X,Y}$	Pearson correlation coefficient between X and Y
σ_X	Standard deviation of variable X

REFERENCES

[1]Areia, C., L. Young, S. Vollam, J. Ede, M. Santos, L. Tarassenko, and P. Watkinson. Wearability testing of ambulatory vital sign monitoring devices: prospective observational cohort study. *JMIR mHealth and uHealth* 8(12):e20214, 2020.

[2]Armstrong, J. S., F. Collopy. Error measures for generalizing about forecasting methods: empirical comparisons. *Int. J. Forecast.* 8(1):69–80, 1992.

[3]Bansal, A., R. Joshi. Portable out-of-hospital electrocardiography: a review of current technologies. *J. Arrhythm.* 34(2):129–138, 2018.

[4]Boddy, R., G. Smith. Statistical Methods in Practice: For Scientists and Technologists. Chicester: Wiley, pp. 95–96, 2009.

[5]Braunstein E., O. Reynbakh, A. Krumerman, L. Di Biase, and K. Ferrick. Inpatient cardiac monitoring using a patch-based mobile cardiac telemetry system during the COVID-19 pandemic. *J. Cardiovasc. Electrophysiol.* 31(11):2803–2811, 2020.

[6]Braunwald, E., P. Z. Douglas, and L. Peter. Heart Disease: A Textbook of Cardiovascular Medicine (6th ed.), Philadelphia: Saunders, 2001.

[7]Dar, T., Y. Bharath, R. Gopinathannair, and D. Lakkireddy. Current advances in wearable health technology: a review. *Electrophysiol. Lab Digest* 18(3), 2018.

[8]Fung, E., M. R. Järvelin, R. N. Doshi, J. S. Shinbane, S. K. Carlson, L. P. Grazette, P. M. Chang, R. S. Sangha, H. V. Huikuri, and N. S. Peters. Electrocardiographic patch devices and contemporary wireless cardiac monitoring. *Front. Physiol.* 6:149, 2015.

[9]Henian, X., G. A. Garcia, and X. Zhao. Automatic detection of ECG electrode misplacement: a tale of two algorithms. *Physiol. Meas.* 33(9):1549, 2012.

[10]Kancharla, K., N. A. M. Estes. Mobile cardiac monitoring during the COVID-19 pandemic: necessity is the mother of invention. *J. Cardiovasc. Electrophysiol.* 31(11):2812–2813, 2020.

[11]Kania, M., H. Rix, M. Fereniec, H. Zavala-Fernandez, D. Janusek, T. Mroczka, G. Stix, and R. Maniewski. The effect of precordial lead displacement on ECG morphology. *Med. Biol. Eng. Comput.* 52(2):109–119, 2014.

[12]Klum, M., T. Minn, T. Tigges, A. G. Pielmus, and R. Orglmeister. Minimally spaced electrode positions for multi-functional chest sensors: ECG and respiratory signal estimation. *Curr. Direct. Biomed. Eng.* 2(1):695–699, 2016.

[13]Lateef, F., A. Annathurai, and T. T. Loh. The V-Quick patch versus the standard 12-lead ECG system: time is the essence. *Int. J. Emerg. Med.* 1(1):43–48, 2008.

[14]Levine, D.M., K. Ouchi, B. Blanchfield, A. Saenz, K. Burke, M. Paz, K. Diamond, C. T. Pu, and J. L. Schnipper. Hospital-level care at home for acutely ill adults a randomized controlled trial. *Ann. Intern. Med.* 172(2):77–85, 2020.

[15]Link M. S., L. C. Berkow, P. J. Kudenchuk, H. R. Halperin, E. P. Hess, V. K. Moitra, R. W. Neumar, B. J. O'Neil, J. H. Paxton, S. M. Silvers, R. D. White, D. Yannopoulos, and M. W. Donnino. Part 7: adult advanced cardiovascular life support: 2015 American Heart Association Guidelines Update for Cardiopulmonary Resuscitation and Emergency Cardiovascular Care. *Circulation* 132(suppl 2):S444–S464, 2015.

[16]Malik, M., J. T. Bigger, A. J. Camm, R. E. Kleiger, A. Malliani, A. J. Moss, and P. J. Schwartz. Heart rate variability: standards of measurement, physiological interpretation, and clinical use. *Eur. heart J.* 17(3):354–381, 1996.

[17]Mckay C. Probability and Statistics, p. 257, 2019. ISBN 9781839473302.

[18]Mittal, S., J. S. Steinberg. Ambulatory external electrocardiographic monitoring: focus on atrial fibrillation. *J. Am. Colloid Cardiol.* 58(17):1741–1749, 2011.

[19]Nallathambi, G., N. Selvaraj, P. L. Rajbhandary. An innovative hybrid approach for detection of pacemaker pulses at low sampling frequency. 42nd Annual International Conference of the IEEE Engineering in Medicine and Biology Society (EMBC), pp. 5012–5015, 2020.

[20]Nasiff CardioCard - PC based Holter ECG System https://nasiff.com/cholter12.pdf. Accessed Oct 4, 2021.

[21]Olson, J. A., A. M. Fouts, B. J. Padanilam, E. N. Prystowksy. Utility of mobile cardiac outpatient telemetry for the diagnosis of palpitations, presyncope, syncope, and the assessment of therapy efficacy. *J. Cardiovasc. Electrophysiol.* 18(5):473–477, 2007.

[22]Powers, D. M. W. Evaluation: from precision, recall and F-measure to ROC, informedness, markedness & correlation. *J. Mach. Learn. Technol.* 2(1):37–63, 2011.

[23]Puurtinen, M., J. Hyttinen, and J. Malmivuo. Optimizing bipolar electrode location for wireless ECG measurement-analysis of ECG signal strength and deviation between individuals. *Int. J. Bioelectromagnet.* 7(1):236–239, 2005.

[24]Puurtinen, M., J. Viik, and J. Hyttinen. Best electrode locations for a small bipolar ECG device: signal strength analysis of clinical data. *Ann. Biomed. Eng.* 37(2):331–336, 2009.

[25]Rajbhandary, P. L., G. Nallathambi. Feasibility of continuous monitoring of core body temperature using chest-worn patch sensor. 42nd Annual International Conference of the IEEE Engineering in Medicine and Biology Society (EMBC), pp. 4652–4655, 2020.

[26]Ramirez, A. H., J. S. Schildcrout, D. L. Blakemore, D. R. Masys, J. M. Pulley, M. A. Basford, D. M. Roden, and J. C. Denny. Modulators of normal electrocardiographic intervals identified in a large electronic medical record. *Heart Rhythm.* 8(2): 272–277, 2011.

[27]Selvaraj, N. Long-term remote monitoring of vital signs using a wireless patch sensor. IEEE Healthcare Innovation Conference (HIC), 2014.

[28]Selvaraj, N., G. Nallathambi, and P. Kettle. A novel synthetic simulation platform for validation of breathing rate measurement. 40th Annual International Conference of the IEEE Engineering in Medicine and Biology Society (EMBC), pp. 1177–1180, 2018.

[29]Selvaraj, N., G. Nallathambi, R. Moghadam, and A. Aga. Fully disposable wireless patch sensor for continuous remote patient monitoring. 40th Annual International Conference of the IEEE Engineering in Medicine and Biology Society (EMBC), pp. 1632–1635, 2018.

[30]Tonino, R. P. B., K. Larimer, O. Eissen, and M. R. Schipperus. Remote patient monitoring in adults receiving transfusion or infusion for hematological disorders using the VitalPatch and accelerateIQ Monitoring System: Quantitative Feasibility Study. *JMIR Hum. Factors* 6(4):e15103, 2019.

[31]Van't Hof, A. W., A. Liem, M.J. de Boer, and F. Zijlstra. Clinical value of 12-lead electrocardiogram after successful

reperfusion therapy for acute myocardial infarction. *The Lancet* 350(9078):615–619, 1997.
[32]VitalConnect Platform: Instruction for Use - VitalPatch Biosensor https://vitalconnect.com/docs/ifu006/revV/IFU-06_Rev_V_VitalPatch_2.0_Instructions_for_Use(final).pdf . Accessed Oct 4, 2021.